The temperature structure of the mesosphere over Taiwan and comparison with other latitudes

Uma Das[1] and C. J. Pan[1]

Received 9 September 2010; revised 11 April 2011; accepted 21 April 2011; published 20 July 2011.

[1] We present here a detailed investigation of the mesospheric temperature structure over Taiwan, a subtropical location, using 9 years of observations (March 2002 to October 2010) by the Sounding of the Atmosphere using Broadband Emission Radiometry (SABER) instrument onboard the Thermosphere-Ionosphere-Mesosphere Energetics and Dynamics (TIMED) satellite. The mesopause (MP) is always found to be located at a higher level with a mean altitude of 98.2 ± 1.8 km and mean temperature of 165.0 ± 5.8 K. The climatological study shows that MP is lower and warmer during summer and higher and cooler during winter, which is different from the midlatitudes and high latitudes as well as from low latitudes. The temperatures of the mesospheric temperature inversions (MTI) and secondary minimum (SM), on the other hand, are lower during summer and higher during winter, and their altitudes do not show any annual variation. It is found that the thermal structure over Taiwan undergoes a phase shift between 89 and 95 km, and above this region it is in phase with the solar flux. Since MP is always above these altitudes, it shows a seasonal variation that is in phase with the solar energy inputs, and the temperatures below (that of MTI and SM) show the opposite seasonal variation caused by mesospheric adiabatic cooling and warming processes.

Citation: Das, U., and C. J. Pan (2011), The temperature structure of the mesosphere over Taiwan and comparison with other latitudes, *J. Geophys. Res.*, *116*, D00P06, doi:10.1029/2010JD015034.

1. Introduction

[2] The mesosphere, which extends from approximately 50 to 100 km, exhibits many interesting phenomena and hence is a very intriguing region of the atmosphere. Primary heating and cooling mechanisms of the mesosphere are mostly in nonlocal thermodynamical equilibrium. Heat input to the mesosphere is through direct solar radiation, chemical heating from exothermic reactions and by collisional quenching. The cooling of mesosphere is through radiative processes, primarily, the infrared emission from CO_2 (at 15 μm), ozone and water vapor. The mesospheric energy budget is also influenced by dynamics through gravity wave breaking, turbulence and adiabatic compressional heating due to vertical motions. Excellent reviews of the subject are available in the literature [*Lindzen*, 1981; *Garcia and Solomon*, 1985; *Hauchecorne et al.*, 1987; *Mlynczak and Solomon*, 1991a, 1991b, 1993; *Roble*, 1995; *Killeen and Johnsson*, 1995; *Meriwether and Mlynczak*, 1995; *Beig et al.*, 2003].

[3] Although the mesosphere is located well above the Earth's surface, its structure can be altered by human activities. Imprints of such changes can be clearly seen in mesospheric chemical composition and temperature. It is difficult to quantify the mesospheric variability due to these effects because of the presence of the much stronger natural sources of variabilities, namely, the seasonal, annual, and solar cycle variations.

[4] The accurate measurement of mesospheric temperature is a challenging problem. Although, a number of methods have been used for temperature measurement, each of these has some merits as well as disadvantages. Some of these methods are hydroxyl airglow, Rayleigh lidar, Na and K lidars, rocket grenades, falling spheres, etc. [*Lübken and von Zahn*, 1991; *Keckhut et al.*, 1995; *Whiteway et al.*, 1995; *von Zahn et al.*, 1996; *She and von Zahn*, 1998; *Leblanc et al.*, 1998; *She et al.*, 2000; *Lübken and Mullemann*, 2003; *Beig et al.*, 2003; *Chu et al.*, 2005; *Beig*, 2006]. All these methods are limited to certain local times and particular locations over the land. A large number of these studies pertain to the Northern Hemisphere and less to the Southern Hemisphere. Also, most of these were for midlatitudes and high latitudes. On the other hand, satellite observations provide a global picture, thereby enabling one to understand the mesosphere and its morphology as a whole [*Thulasiraman and Nee*, 2002; *Shepherd et al.*, 2004; *Xu et al.*, 2007; *Kishore Kumar et al.*, 2008; *Venkat Ratnam et al.*, 2010]. Using daytime zonally averaged temperatures from the Wind Imaging Interferometer (WINDII) instrument onboard the Upper Atmosphere Research Satellite (UARS) for the period 1991–1997, the global variability of mesospheric temperature was investigated in detail at three altitudes: 75, 82 and 87 km [*Shepherd et al.*, 2004]. A strong semiannual oscillation in equatorial and tropical latitudes and dominant annual (winter maximum and summer minimum), 90 day and 60 day

[1]Institute of Space Science, National Central University, Jhongli, Taiwan.

oscillations in midlatitudes and high latitudes were observed. A quasi-biennial oscillation (QBO) was also observed extending from 45°S to 65°N.

[5] The mesopause (hereinafter referred to as MP), now considered more as a region than a layer [*Beig et al.*, 2003], is the coldest part of the atmosphere. Using shipborne lidar measurements during April–July 1996, *von Zahn et al.* [1996] showed that there are two distinct levels of MP altitude on the global scale and that MP was lower (86 ± 3 km) and cooler (150–170 K) in the northern midlatitudes and high latitudes and higher (100 ± 3 km) and warmer (160–190 K) at the other latitudes. Investigation of temperature data for MP characteristics from the High Resolution Doppler Imager (HRDI) instrument onboard the UARS satellite also revealed a lower and cooler MP during summer and a higher and warmer MP in winter [*Thulasiraman and Nee*, 2002; *Venkat Ratnam et al.*, 2004]. *Xu et al.* [2007] also got the same results for MP characteristics using the observations of the Sounding of the Atmosphere using Broadband Emission Radiometry (SABER) onboard the Thermosphere-Ionosphere-Mesosphere Energetics and Dynamics (TIMED) satellite during 2002–2006. The switch over from the summer-type MP to the winter-type MP takes place in 30°–40° latitude. In addition, MP characteristics are also strongly modulated by the diurnal and the semidiurnal tides at all latitudes. Many ground-based measurements from midlatitudes and high latitudes also showed the presence of the two-level MP [*Leblanc et al.*, 1998; *She and von Zahn*, 1998; *States and Gardner*, 2000; *She et al.*, 2000]. At the equator and tropical latitudes, MP is at the higher altitude during all seasons with no significant variations [*Xu et al.*, 2007; *Kishore Kumar et al.*, 2008; *Venkat Ratnam et al.*, 2010].

[6] The mesospheric inversion layer or the mesospheric temperature inversion (hereinafter called MTI), first observed by *Schmidlin* [1976] in temperature profiles measured using falling spheres and acoustic grenades, is another interesting phenomenon in the mesosphere [*Meriwether and Gardner*, 2000]. In low latitudes and midlatitudes MTIs were observed with great regularity in both upper mesosphere (60–70 km) and the MP region (90–100 km). Majority of the studies on MTIs have been conducted from midlatitudes based on Rayleigh and Na lidar measurements [*Hauchecorne et al.*, 1987; *Whiteway et al.*, 1995; *Leblanc and Hauchecorne*, 1997; *She et al.*, 2000; *States and Gardner*, 2000; *Chu et al.*, 2005, etc.] and a few studies from the low latitudes [*Siva Kumar et al.*, 2001; *Venkat Ratnam et al.*, 2002]. Using the measurements from two midlatitude stations in France, Observatoire de Haute-Provence (OHP, 44°N, 5°E) and Centre d'Essais des Landes (CEL, 44°N, 1°W), *Hauchecorne et al.* [1987] showed that the altitude of MTI has an annual variation occurring in 70–83 km during summer and at further lower altitudes during winter. The altitude of the secondary minimum, which is the temperature minimum below the inversion layer (following the terminology of *Hauchecorne et al.* [1987] and hereinafter referred to as SM), also follows an annual variation.

[7] Studies on mesospheric temperature structure over subtropical latitudes have been very few. Using Na lidar measurements *Clemesha et al.* [1999] showed that MP temperature and altitude over a subtropical station, Sao Jose dos Campos (23°S, 46°W), Brazil, during July to October 1998 were 190 K and 103 km, respectively. *Leblanc et al.* [1998] showed from Rayleigh lidar measurements over Mauna Loa (MLO; 19.5°N, 155.6°W), Hawaii that the mesosphere follows a semiannual cycle under the influence of the equatorial dynamics and is also modulated by the midlatitude annual cycle. *Friedman and Chu* [2007] discussed the seasonal variations of the nocturnal thermal structure of the mesosphere over Arecibo observatory (18.35°N, 66.75°W) using K lidar measurements. All these studies pertain to the nighttime and thus carry tidal signatures. A proper diurnal averaging is very important to understand accurately the seasonal variations and climatological features of the mesospheric thermal structure. Such an opportunity is provided by satellite measurements. In addition, a long database will enhance the statistical significance of the climatology. The present study aims to bridge the gap between the current understanding of mesosphere over low latitudes and that over midlatitudes and high latitudes by investigating the temperature structure of mesosphere over Taiwan (centered at 24°N, 121°E), a subtropical region in the Northern Hemisphere. We have used the temperature data retrieved from the measurements of the SABER instrument to investigate in complete detail the climatology and other long-period variations in the altitudes and temperatures of MP, MTI, SM, and the subtropical mesosphere in general.

2. Data and Analysis

[8] The TIMED satellite was launched in December 2001 in a Sun-synchronous polar orbit at 625 km with an inclination of 74.1°. The satellite makes ~15 orbits per day with a period of 1.6 h and takes 60 days to complete a full 24 h cycle in local time. SABER is one of the four instruments on the TIMED satellite whose aim is to advance the understanding of the structure, energetics, chemistry and dynamics of the atmosphere from 20 to 120 km. SABER measures the Earth limb emissions in 10 broadband radiometer channels ranging from 1.27 μm to 17 μm. The kinetic temperature from the tropopause to the lower thermosphere is retrieved from CO_2 15 μm limb emission using a full nonlocal thermal equilibrium (non-LTE) inversion method [*Mertens et al.*, 2001, 2004].

[9] In the present study we have used the SABER 2A level data product of version 1.07 from March 2002 to October 2010, a little less than 9 years of data. To investigate the mesosphere over Taiwan, we considered a latitude-longitude grid of 6° × 4° covering 21°N–27°N and 119°E–123°E region. Figure 1 shows a map of Taiwan and highlights the region of interest in the present study by a thick black box.

[10] *Mertens et al.* [2001] have documented the retrieval uncertainties to be 1.4 K at 80 km, 7.8 K at 100 km and 22.5 K at 110 km for the early versions of the temperature data from the SABER instrument. *Remsberg et al.* [2008] have shown from their comparison of the latest 1.07 version temperatures with other ground-based observations that the error was within about ±5 K and concluded that the temperatures of this version, in the upper mesosphere and lower thermosphere region, are of good quality. Considering the errors in the non-LTE parameters, *García-Comas et al.* [2008] showed that the overall error in these temperatures is

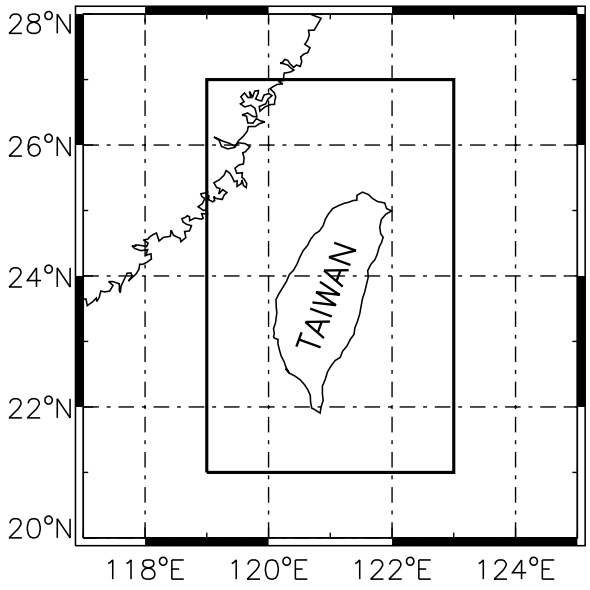

Figure 1. Map showing the grid in which the SABER/TIMED observations have been considered in the present study to investigate the mesosphere over Taiwan.

around ±1–2 K below 95 km and ±4 K at 100 km. The errors are larger when the temperature profiles have pronounced vertical structure, i.e., strong temperature inversion layers, and can rise up to ±3 K around 80 km and ±8 K at 90 km. The vertical resolution of the SABER temperature profiles is ~2 km [*Mertens et al.*, 2004].

[11] Each individual SABER temperature profile is smoothed using Chebeshyv polynomials with a cut off wavelength of 4 km to remove the short-scale gravity wave features and for the accurate identification of MP, MTI, and SM. The temperatures and altitudes of MP, MTI and SM are identified from each profile and the climatological properties investigated. SABER takes 60 days to cover all local times at a particular location. However, observations around local noon are mostly absent. The temperatures and altitudes of MP, MTI, and SM of every 2 months are sorted in local time and a least squares fit for 24, 12 and 8 h harmonics is performed. The constants obtained from these fits are used to compute the diurnal series for every 2 months and averaged to obtain the bimonthly mean temperatures and altitudes. This process removes the tidal effects, but the effects of planetary-scale waves may still exist in the averages. Similarly, to investigate the mesospheric temperature structure, the temperature profiles of every 2 months are sorted in local time and a least squares fit for 24, 12 and 8 h harmonics is performed at each altitude level. The constants obtained from these fits are used to compute the diurnal temperature series for every 2 months and averaged to obtain the bimonthly mean profile. The months are grouped as JF (January–February), MA (March–April), MJ (May–June), JA (July–August), SO (September–October), and ND (November–December). Since we are interested in the long-period variations and the climatological behavior of the mesospheric temperature structure over Taiwan, sorting the data at finer temporal scales is not required. Figure 2 shows a histogram of the number of temperature profiles available in the Taiwan grid during the bimonthly periods from March 2002 to October 2010. The total number of profiles available is 1874 and the average number of profiles is 36 per 2 months.

[12] A harmonic analysis is also performed on the altitudes and temperatures of MP, MTI and SM using the continuous wavelet transform (CWT) [*Farge*, 1992; *Torrence and Compo*, 1998] and the fast Fourier transform (FFT). Spectral analysis tools are very important in understanding the periodic variations of different parameters in observational sciences. The most popular till date is the FFT, which is useful for spectral analysis of linear and stationary data. However, seldom are geophysical data sets linear and stationary. The wavelet transform provides an advancement as it is capable of analyzing nonstationary data and gives time-frequency localization [*Farge*, 1992; *Torrence and Compo*, 1998]. The wavelet transform, relative to some basic wavelet, provides a flexible time frequency window which automatically narrows when observing high-frequency components and widens when observing low-frequency components. The technique of using wavelets to identify localized power events in time series is now being used and applied in various geophysical studies [e.g., *Das and Sinha*, 2008; *Das et al.*, 2009].

[13] For a discrete equally spaced time series x_n (like in the data set used in the present study), where $n = 0, 1, \ldots N - 1$ is the index in time, the convolution of x_n with a scaled and translated version of ψ gives the continuous wavelet transform:

$$W_n(s) = \sum_{n'=0}^{N-1} x_{n'} \psi^* \left[\frac{(n' - n)\delta t}{s} \right] \quad (1)$$

[14] By varying the wavelet scale s and translating along the localized time index n, the wavelet coefficients can be computed. The wavelet power spectrum, also called spectrogram, is defined as $|W_n(s)|^2$. The software written in IDL, provided by *Torrence and Compo* [1998] is used in the present analysis. The Morlet wavelet, which is a plane wave

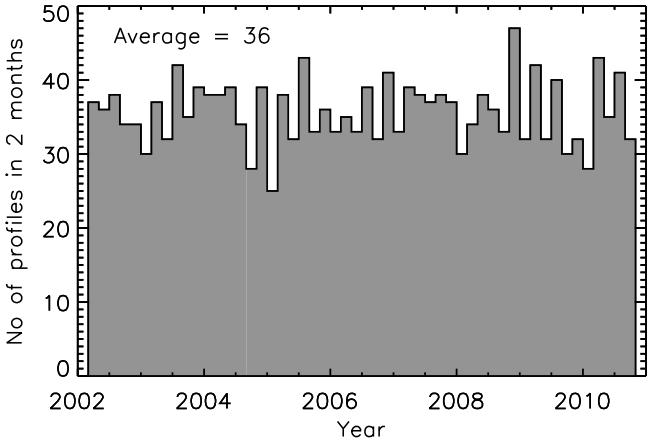

Figure 2. A histogram showing the number of available temperature profiles from SABER during the bimonthly periods from March 2002 to October 2010. The average number of profiles per 2 months is 36.

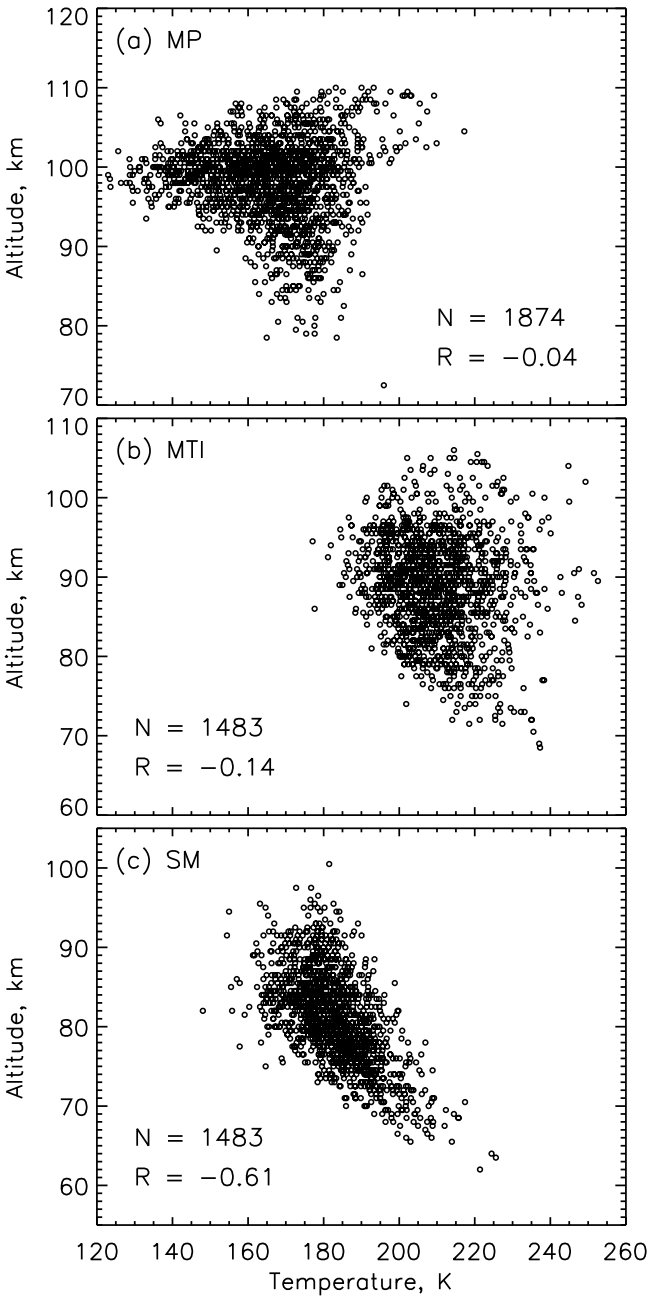

Figure 3. A scatterplot of the temperature versus altitude of (a) MP, (b) MTI, and (c) SM, obtained from all the individual profiles observed by SABER instrument in the Taiwan grid shown in Figure 1. The number of data points (N) for MTI and SM was reduced as we applied the definition of *Hauchecorne et al.* [1987] to establish the existence of a temperature inversion when investigating individual profiles. R is the correlation coefficient. See text for more details.

modulated by a Gaussian, is used for computing the wavelet coefficients. It is a complex wavelet and is given as

$$\psi_0(\eta) = \pi^{-1/4} e^{i\omega_0\eta} e^{-\eta^2/2} \quad (2)$$

where η is a dimensionless time parameter and ω_0 is the frequency, here taken to be 6 to satisfy the admissibility condition. The technique is described in detail by *Farge* [1992] and *Torrence and Compo* [1998].

3. Mesospheric Parameters and the Long-Period Variations

[15] Each individual temperature profile available in the Taiwan grid is investigated to identify MP, MTI, and SM. Figure 3 shows a scatterplot of the altitude versus temperature of these three features. MP is identified from all the available 1874 temperature profiles and Figure 3a shows that most of the MPs are concentrated around 100 km, although there is a large variation in the temperature. The MPs at other altitudes are less in number and the variation in temperature is also low. There is no correlation between the altitude and temperature of MP (correlation coefficient, $R = -0.04$). For the identification of SM and MTI in the individual profiles, we used the definition of *Hauchecorne et al.* [1987], according to which, it is considered that an inversion layer exists if the increase above the secondary minimum is greater than 10 K. With this criterion, only 1483 profiles, spread almost uniformly over the 9 year period under study, showed the presence of an MTI and a corresponding SM. Figure 3b shows the distribution of the MTI altitude versus temperature. It can be seen that the MTIs are spread over a wide range of altitudes from 70 to 100 km and temperatures from 180 to 240 K and the overall correlation between MTI altitude and the temperature is very low ($R = -0.14$). Figure 3c shows the same for SM and it can be seen that the distribution is confined to higher temperatures at lower altitudes and vice versa. The correlation coefficient between the altitude of SM and the temperature is −0.61, showing a strong anticorrelation in comparison to that of MP and MTI. This could be due to the simple fact that the average lapse rate in the mesosphere is positive and one finds higher temperatures at lower altitudes. However, there are many factors contributing to the formation and sustenance of these features in the mesosphere [*Lindzen*, 1981; *Hauchecorne et al.*, 1987; *Meriwether and Mlynczak*, 1995; *Meriwether and Gardner*, 2000].

[16] Bimonthly mean altitudes and temperatures are computed using the procedure described in section 2. The mean MP altitude and temperature during the study period are 98.2 ± 1.8 km and 165.0 ± 5.8 K, respectively. The mean MTI and SM altitudes are 87.0 ± 2.2 km and 80.0 ± 2.0 km, respectively, showing that the MTIs are occurring mostly at the higher altitudes over Taiwan. The mean MTI and SM temperatures are 207.0 ± 3.8 K and 184.9 ± 4.0 K, respectively. The bimonthly mean altitudes and temperatures of MP, MTI, and SM showed significant seasonal variations and were subjected to the continuous wavelet transform. A linear regression line was first subtracted from each data series to remove the DC component and normalized to the standard deviation of the same. The CWT, described earlier, was applied to each of them. Figure 4 (left) shows the wavelet spectrograms of the altitudes and those of the temperatures are shown in Figure 4 (right). In Figure 4, the top, middle, and bottom plots are for MP, MTI, and SM, respectively. The solid and the dotted contours around the high-power islands are the 95% and the 80% confidence levels, respectively. The thick solid black line is the "cone of influence" beyond which the wavelet coefficients are subject to errors due to

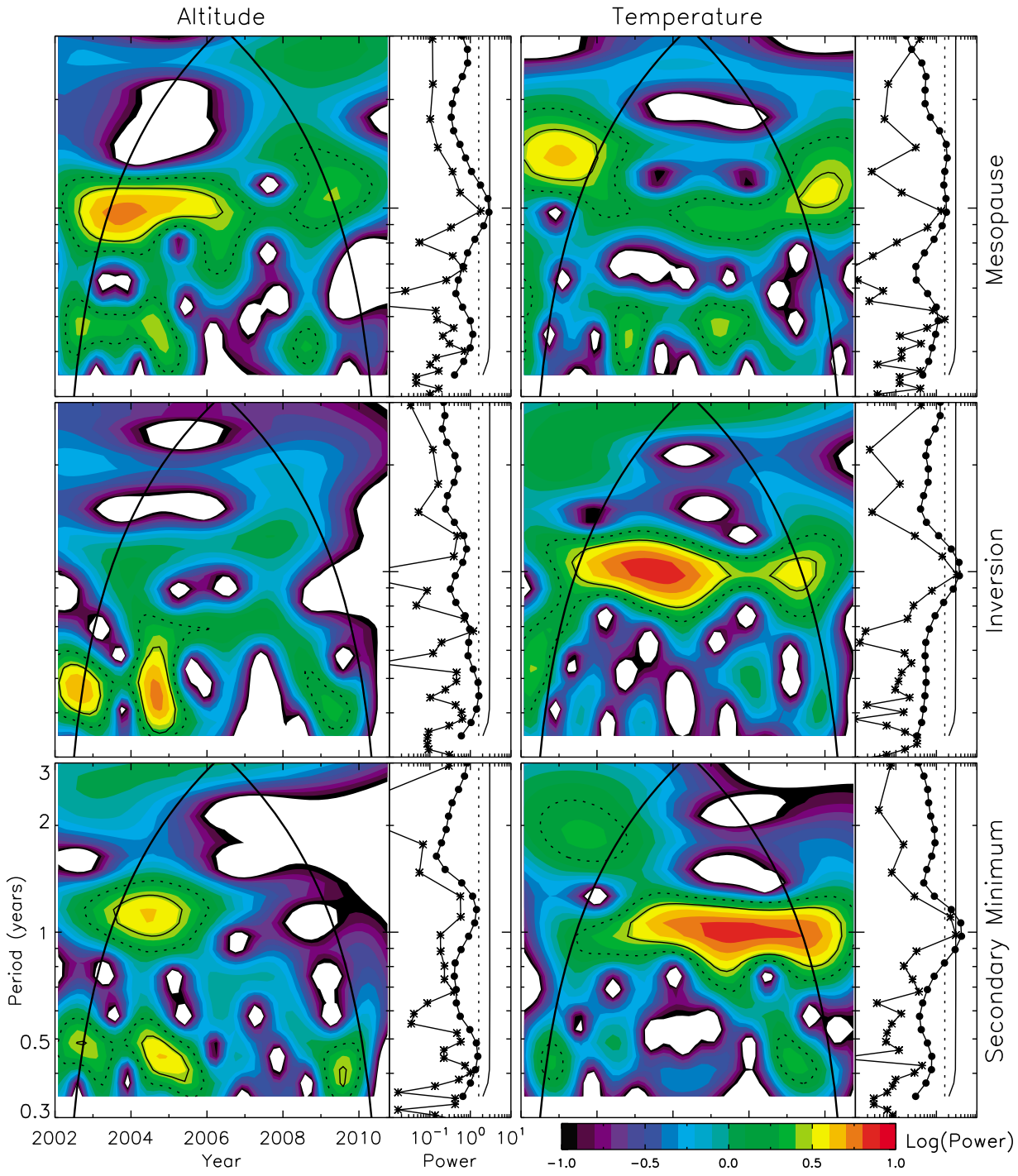

Figure 4. Wavelet spectrograms of the (left) altitudes and (right) temperatures of (top) MP, (middle) MTI, and (bottom) SM. The thin solid and dotted contours surrounding the high-power green to red islands are the 95% and 80% confidence levels, respectively. The thick solid black line is the cone of influence beyond which the wavelet coefficients are subject to errors. The vertical plot to the right of each spectrogram shows the global power spectrum and also the Fourier spectrum along with the 95% and 80% confidence levels. Observe the strong annual variations in the MTI and SM temperatures.

edge effects and are not completely reliable. They are, therefore, not discussed hereinafter. The vertical plot beside each spectrogram shows the global power spectrum (solid circles), which is the time-averaged wavelet power, and also the Fourier power spectrum (stars) of the corresponding data series. The 95% and the 80% confidence levels are shown in the vertical plots in Figure 4 also by solid and dotted lines, respectively.

[17] The wavelet spectrogram of MP altitude shows a statistically significant annual variation from 2002 to 2006. The global power spectrum and the Fourier spectrum also show that there is a significant annual variation in MP

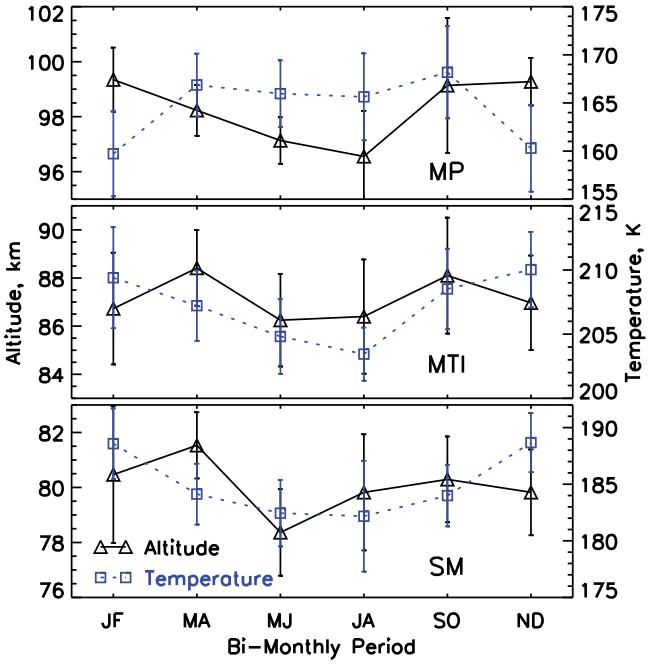

Figure 5. The bimonthly climatology of the altitudes and temperatures of (top) MP, (middle) MTI, and (bottom) SM.

altitude and the average amplitude of variation is ±1.5 km. An investigation of the phases shows that the altitude is lower during summer and higher during winter. There is also a less significant semiannual oscillation during 2002–2005 and 2008. The wavelet spectrogram of MP temperature shows a statistically less significant annual oscillation from 2006 to 2009. The phases show that MP temperature is high during summer and low during winter and the average amplitude of variation is ±4 K. Also, a statistically less significant semiannual variation is present during 2004–2005 and 2007. The phases show that the temperature is high during equinoxes and low during solstices. The global power spectra and the Fourier spectra of both MP temperature and altitude show that the annual variation is dominant, followed by the semiannual variation. Figure 5 (top, middle, and bottom) shows the climatology obtained from the bimonthly mean altitudes and temperatures of MP, MTI, and SM, respectively. The MP altitude and temperature in Figure 5 (top) show annual variations with a lower and warmer MP in summer and higher and cooler MP in winter. The presence of a statistically less significant semiannual variation with maxima during the equinoxes has resulted in slightly higher temperatures during MA and SO months. These variations are similar to those observed in the wavelet spectrograms. The altitude of MP over Gadanki (13.5°N, 79.2°E), a tropical latitude location in India, was also around 98 km, but did not show any significant seasonal variation and the MP temperature was fluctuating between 178 and 195 K, with no particular seasonal variation [*Venkat Ratnam et al.*, 2010]. In contrast, MP altitude and temperature over Taiwan are showing small but significant seasonal variations. These variations and the amplitudes of variation are in accordance with the earlier study by *Xu et al.* [2007]. Similar results were obtained by *Chu et al.* [2005] over Maui, Hawaii (20.7°N) for the MP characteristics using the NRLMSIS-00 model [*Picone et al.*, 2002]. Their results showed that the MP altitude in winter was around 99 km and around 96 km in summer, with a smooth transition. Their observations using a Na lidar, however, showed a summer minimum of 87.5 km. At Arecibo observatory also, MP temperature was found to be similar to midlatitude variation with a winter high and summer low [*Friedman*, 2003]. It should be remembered that all these observations were limited to nighttime.

[18] The altitudes of MTI and SM show statistically significant semiannual variations during 2002–2005 and 2009 in Figure 4. SM altitude shows a statistically significant annual variation only during 2004–2005. The global power spectra also show that both peaks are prominent in SM altitude, while only the semiannual peak is prominent in MTI altitude. The MTI and SM temperatures show statistically significant annual oscillations almost throughout the entire period of study. The global power spectra also show that the annual oscillation is the most dominant. An investigation of the phases shows that both temperatures are high during winter and low during summer, and this seasonal variation is exactly opposite to that seen in MP temperature. Figure 5 also shows that the MTI and the SM temperatures are high during winter and low during summer, in accordance with the results obtained from the wavelet analysis. The altitudes show a semiannual variation with maxima during MA and SO months. Wavelet analysis also showed the same results. The SM temperature over Gadanki also showed similar seasonal behavior and the SM altitude, while showing a semiannual variation, peaked during the solstices [*Venkat Ratnam et al.*, 2010]. However, SM was more prominent during equinoxes in comparison to solstices. At midlatitudes, the altitude of SM showed annual variation with maximum during summer and minimum during winter [*Hauchecorne et al.*, 1987; *Leblanc and Hauchecorne*, 1997].

4. Variations in the Subtropical Mesosphere

[19] Bimonthly climatological profiles obtained by averaging the bimonthly mean profiles of all years are shown in Figure 6. The profile for JF months shows the actual values and each successive profile is shifted by 20 K for proper visualization. The last profile shown by the thick solid line is the average of all bimonthly mean profiles during the 9 year period. Significant variations can be observed among the bimonthly profiles with pronounced differences in the mesosphere and MP. It should be remembered that we have computed the bimonthly profiles by averaging over all local times, and in spite of this analysis procedure, the MTI at around 88 km seems to be a prominent feature in the climatological profiles as well as in the 9 year mean, albeit with less amplitude. The MTIs are broader and discernible during equinoxes; narrower and discernible during summer and not very distinguishable in winter. This is similar to the climatology observed over Gadanki. However, the climatological mean over Taiwan is different from the long-term mean obtained over Gadanki, where the temperature was nearly constant in the 75–90 km region [*Venkat Ratnam et al.*, 2010].

[20] To further understand the long-term behavior of the mesospheric temperature structure over Taiwan, the devia-

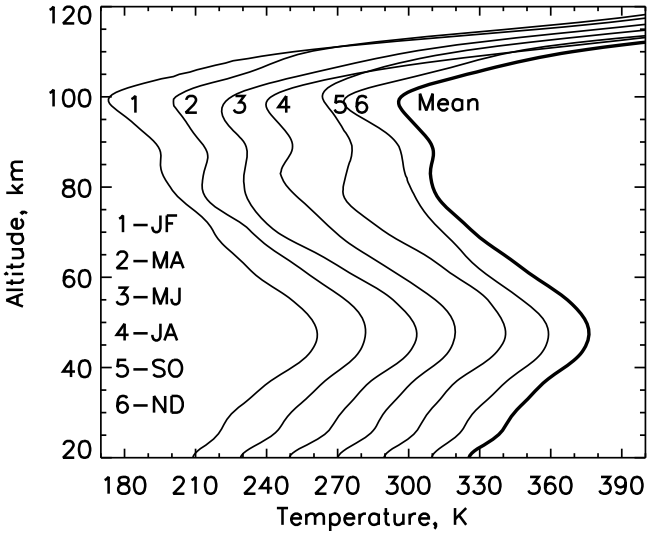

Figure 6. The climatology of the bimonthly mean temperatures observed over Taiwan. The January–February profile shows the actual values, and each successive profile is shifted by 20 K for better visualization. The last profile, shown by the thick solid line, is the mean of all bimonthly means during the 9 year period. Observe the small inversion feature at 88 km that is present in all the profiles, including the 9 year mean profile.

tions of the bimonthly means from the 9 year climatological mean are computed and shown in Figure 7. Grid lines are also plotted in Figure 7 to aid the eye. The annual oscillations seem to be dominant at almost all altitudes. The temperatures are higher in winter and lower in summer in the upper mesosphere. At around 95 km, a semiannual oscillation is present with solstice minima and equinoctial maxima. Above this altitude, the annual variation is once again the dominant variation with a phase shift. The temperatures are showing the opposite seasonal variation with cooler winters and warmer summers. To understand these variations, a least squares fit of 2 year (quasi-biennial oscillation), 1 year (annual oscillation) and half-year (semiannual oscillation) harmonics was performed on the temperature fluctuations at each altitude. Figure 8 (left and middle) shows the amplitudes and phases of the three oscillations obtained from these fits, and Figure 8 (right) shows the correlation coefficients of the fits as a function of altitude. The fits are not good at 73.0, 86.0, and 90.5 km. It is important to note that the amplitude of the annual oscillation is the largest at all altitudes except around 95 km, where the amplitude of semiannual oscillation dominates. The phase of the annual oscillation starts gradually changing at 89 km and undergoes a shift of 180° by 95 km and remains constant above. The semiannual oscillation also undergoes phase shifts at 80 and 102 km. Between 80 and 102 km, the semiannual oscillation shows solstice minima and equinox maxima and above and below this region it shows the opposite variations. Also, the correlation coefficient is less than 0.6 from 89 to 95 km, where the phase of the annual oscillation is changing. Such a phase shift in the annual oscillation was observed by *Chu et al.* [2005] over Maui in both observations and model results. *Shepherd et al.* [2004] also observed a similar phase reversal in the semiannual oscillation over equatorial and tropical latitudes with solstice maxima and equinox minima at 75 km and the opposite at 87 km. This is similar to the semiannual phases observed in the present study.

[21] Over midlatitudes and high latitudes MP is cooler and around 86 km during summer and warmer and at 95–100 km during winter [*von Zahn et al.*, 1996; *She and von Zahn*, 1998; *States and Gardner*, 2000; *She et al.*, 2000; *Thulasiraman and Nee*, 2002; *Xu et al.*, 2007]. Two processes compete to define MP and result in such a seasonal variation at these latitudes. In summer, there is strong adiabatic cooling caused by the mean upward velocities below ~91 km and the annual trend at these heights is cool summer and warm

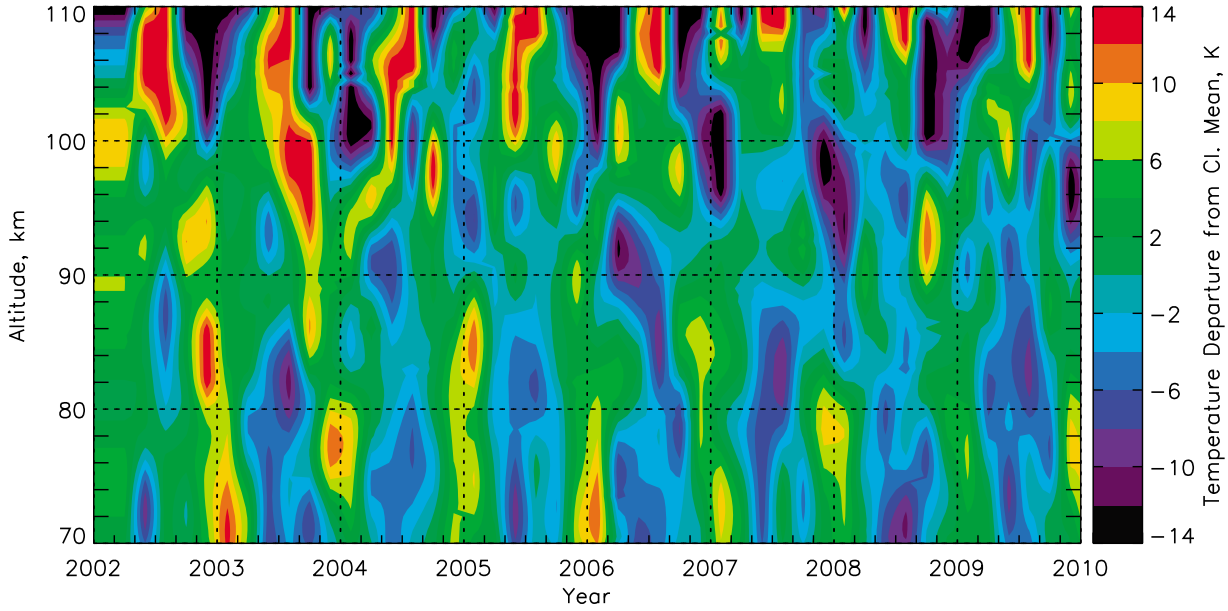

Figure 7. The temperature deviations from the 9 year climatological mean. Observe the change in phase of the annual oscillation between 89 and 95 km.

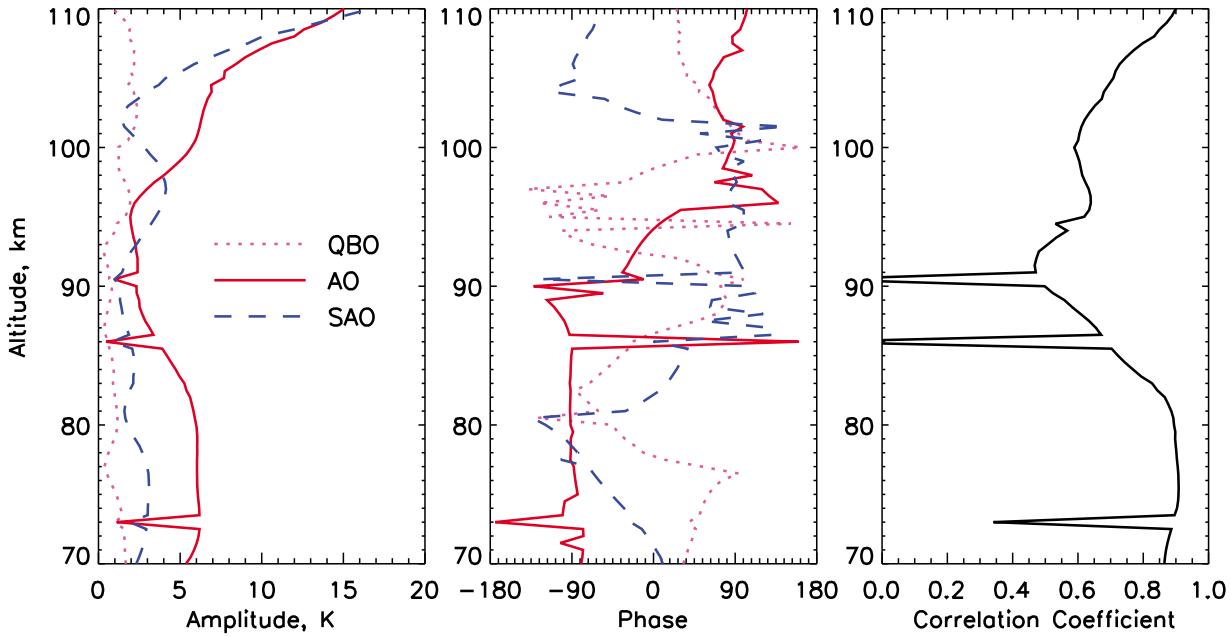

Figure 8. (left) Amplitudes and (middle) phases of the quasi-biennial, annual, and semiannual oscillations from the least squares fitting and (right) the correlation coefficients of the fits as a function of altitude.

winter. Above 98 km, there is increased UV absorption by O_2 during summer resulting in high temperatures and decreased absorption in winter resulting in low temperatures. Hence, there are two local minima in the temperature, and MP is defined as the lower of these two. In summer, adiabatic cooling is very strong and thus, MP drops down to lower altitudes at ~87 km, and during winter, the higher-altitude minimum in 95–100 km, defines the same [*States and Gardner*, 2000]. In comparison, MP altitude over subtropical latitudes is limited to the upper level and unlike the steady MP at equatorial and tropical latitudes [*Xu et al.*, 2007; *Kishore Kumar et al.*, 2008; *Venkat Ratnam et al.*, 2010] the subtropical MP shows significant seasonal variations albeit with less amplitude. The warm summer and cool winter MP, is due to the solar energy inputs and is not affected by the mesospheric dynamics below. However, the MTI and the SM are affected and hence, we observe the opposite seasonal variation in their temperatures. This is supported by the phase reversal observed in Figure 8 at ~88 km and explains the seasonal variations observed in all the temperatures in section 3. The adiabatic cooling and warming processes in the lower altitudes exist at the subtropical latitudes also, but are not strong enough to bring down the MP.

5. Summary

[22] The temperature structure of mesosphere over Taiwan, a subtropical station, is investigated using observations by the SABER instrument onboard the TIMED satellite during the period from March 2002 to October 2010. The study reveals some interesting features that are different from the midlatitudes and high latitudes as well as from the low latitudes.

[23] 1. MP altitude is confined to the upper level; the average altitude is 98.2 ± 1.8 km.

[24] 2. MP altitude and temperature show significant annual variation with lower and warmer MP in summer and higher and cooler MP in winter. The amplitude of variation of MP altitude is only ±1.5 km and that of the temperature is ±4 K. This seasonal variation is in phase with the solar flux, showing that the MP over subtropical latitudes is controlled by the solar energy inputs.

[25] 3. MTI and SM altitudes are showing weak semiannual oscillations and their temperatures are showing significant annual oscillations being high during winter and low during summer. Such a seasonal variation in the temperature is the result of adiabatic warming and cooling processes in the mesosphere that are in opposite phase to the solar energy inputs.

[26] 4. A phase jump in the annual variation occurring between 89 km and 95 km is observed in accordance with earlier studies. This explains the opposite seasonal variations in the mesosphere (MTI and SM) temperatures and MP temperature.

[27] **Acknowledgments.** The authors acknowledge the SABER/TIMED team for providing free access to the temperature data. U.D. and C.J.P. are supported by the NSC of Taiwan through grant NSC 99-2111-M-008-006-MY2. The authors thank all the reviewers for their valuable suggestions in improving the manuscript.

References

Beig, G. (2006), Trends in the mesopause region temperature and our present understanding—An update, *Phys. Chem. Earth*, *31*, 3–9, doi:10.1016/j.pce.2005.03.007.

Beig, G., et al. (2003), Review of mesospheric temperature trends, *Rev. Geophys.*, *41*(4), 1015, doi:10.1029/2002RG000121.

Chu, X., C. S. Gardner, and S. J. Franke (2005), Nocturnal thermal structure of the mesosphere and lower thermosphere region at Maui, Hawaii (20.7°N), and Starfire Optical Range, New Mexico (35°N), *J. Geophys. Res.*, *110*, D09S03, doi:10.1029/2004JD004891.

Clemesha, B. R., I. Veselovskii, P. P. Batista, M. P. Jorge, and D. M. Simonich (1999), First mesopause temperature profiles from a fixed

Southern Hemisphere site, *Geophys. Res. Lett.*, *26*, 1681–1684, doi:10.1029/1999GL900342.

Das, U., and H. S. S. Sinha (2008), Long term variations in oxygen green line emission over Kiso, Japan from ground photometric observations using continuous wavelet transform, *J. Geophys. Res.*, *113*, D19115, doi:10.1029/2007JD009516.

Das, U., H. S. S. Sinha, S. Sharma, H. Chandra, and S. K. Das (2009), Fine structure of the low-latitude mesospheric turbulence, *J. Geophys. Res.*, *114*, D10111, doi:10.1029/2008JD011307.

Farge, M. (1992), Wavelet transforms and their applications to turbulence, *Annu. Rev. Fluid Mech.*, *24*, 395–458 doi:10.1146/annurev.fl.24.010192.002143.

Friedman, J. S. (2003), Tropical mesopause climatology over the Arecibo Observatory, *Geophys. Res. Lett.*, *30*(12), 1642, doi:10.1029/2003GL016966.

Friedman, J. S., and X. Chu (2007), Nocturnal temperature structure in the mesopause region over the Arecibo Observatory (18.35°N, 66.75°W): Seasonal variations, *J. Geophys. Res.*, *112*, D14107, doi:10.1029/2006JD008220.

Garcia, R. R., and S. Solomon (1985), The effect of breaking gravity waves on the dynamics and chemical composition of the mesosphere and lower thermosphere, *J. Geophys. Res.*, *90*, 3850–3868, doi:10.1029/JD090iD02p03850.

García-Comas, M., et al. (2008), Errors in Sounding of the Atmosphere using Broadband Emission Radiometry (SABER) kinetic temperature caused by non-local-thermodynamic-equilibrium model parameters, *J. Geophys. Res.*, *113*, D24106, doi:10.1029/2008JD010105.

Hauchecorne, A., M. L. Chanin, and R. Wilson (1987), Mesospheric temperature inversion and gravity wave breaking, *Geophys. Res. Lett.*, *14*, 933–936, doi:10.1029/GL014i009p00933.

Keckhut, P., A. Hauchecorne, and M. L. Chanin (1995), Midlatitude long-term variability of the middle atmosphere: Trends and cyclic and episodic changes, *J. Geophys. Res.*, *100*, 18,887–18,897, doi:10.1029/95JD01387.

Killeen, T. L., and R. M. Johnsson (1995), Upper atmospheric waves, turbulence, and winds: Importance for mesospheric and thermospheric studies, *Rev. Geophys.*, *33*(S1), 737–744.

Kishore Kumar, G., M. Venkat Ratnam, A. K. Patra, S. Vijaya Bhaskara Rao, and J. Russell (2008), Mean thermal structure of the low-latitude middle atmosphere studied using Gadanki Rayleigh lidar, Rocket, and SABER/TIMED observations, *J. Geophys. Res.*, *113*, D23106, doi:10.1029/2008JD010511.

Leblanc, T., and A. Hauchecorne (1997), Recent observations of mesospheric temperature inversions, *J. Geophys. Res.*, *102*, 19,471–19,482, doi:10.1029/97JD01445.

Leblanc, T., I. S. McDermid, P. Keckhut, A. Hauchecorne, C. Y. She, and D. A. Krueger (1998), Temperature climatology of the middle atmosphere from long-term lidar measurements at middle and low latitudes, *J. Geophys. Res.*, *103*, 17,191–17,204, doi:10.1029/98JD01347.

Lindzen, R. S. (1981), Turbulence and stress owing to gravity wave and tidal breakdown, *J. Geophys. Res.*, *86*, 9707–9714, doi:10.1029/JC086iC10p09707.

Lübken, F. J., and A. Mullemann (2003), First in situ temperature measurements in the summer mesosphere at very high latitudes (78°N), *J. Geophys. Res.*, *108*(D8), 8448, doi:10.1029/2002JD002414.

Lübken, F. J., and U. von Zahn (1991), Thermal structure of the mesopause region over polar latitudes, *J. Geophys. Res.*, *96*, 20,841–20,857, doi:10.1029/91JD02018.

Meriwether, J. W., and C. S. Gardner (2000), A review of the mesosphere inversion layer phenomenon, *J. Geophys. Res.*, *105*, 12,405–12,416, doi:10.1029/2000JD900163.

Meriwether, J. W., and M. G. Mlynczak (1995), Is chemical heating a major cause of the mesosphere inversion layer?, *J. Geophys. Res.*, *100*, 1379–1387, doi:10.1029/94JD01736.

Mertens, C. J. G. M., M. L. Puertas, P. P. Wintersteiner, R. H. Picard, J. R. Winick, L. L. Gordley, and J. M. R. I. I. Ih (2001), Retrieval of mesospheric and lower thermospheric kinetic temperature from measurements of CO_2 15 μm Earth limb emission under non-LTE conditions, *Geophys. Res. Lett.*, *28*, 1391–1394, doi:10.1029/2000GL012189.

Mertens, C. J., et al. (2004), SABER observations of mesospheric temperatures and comparisons with falling sphere measurements taken during the 2002 summer MaCWAVE campaign, *Geophys. Res. Lett.*, *31*, L03105, doi:10.1029/2003GL018605.

Mlynczak, M. G., and S. Solomon (1991a), Middle atmosphere heating by exothermic chemical reactions involving odd-hydrogen species, *Geophys. Res. Lett.*, *18*, 37–40, doi:10.1029/90GL02672.

Mlynczak, M. G., and S. Solomon (1991b), On the efficiency of solar heating in the middle atmosphere, *Geophys. Res. Lett.*, *18*, 1201–1204, doi:10.1029/91GL01525.

Mlynczak, M. G., and S. Solomon (1993), Detailed evaluation of the heating efficiency in the middle atmosphere, *J. Geophys. Res.*, *98*, 10,517–10,541, doi:10.1029/93JD00315.

Picone, J. M., A. E. Hedin, D. P. Drob, and A. C. Aikin (2002), NRLMSISE-00 empirical model of the atmosphere: Statistical comparisons and scientific issues, *J. Geophys. Res.*, *107*(A12), 1468, doi:10.1029/2002JA009430.

Remsberg, E. E., et al. (2008), Assessment of the quality of the version 1.07 temperature-versus-pressure profiles of the middle atmosphere from TIMED/SABER, *J. Geophys. Res.*, *113*, D17101, doi:10.1029/2008JD010013.

Roble, R. G. (1995), *Energetics of the mesosphere and thermosphere*, in *The Upper Mesosphere and Lower Thermosphere: A Review of Experiment and Theory*, *Geophys. Monogr. Ser.*, vol. 87, edited by R. M. Johnson and T. L. Killeen, pp. 1–22, AGU, Washington, D. C.

Schmidlin, F. J. (1976), Temperature inversions near 75 km, *Geophys. Res. Lett.*, *3*, 173–176, doi:10.1029/GL003i003p00173.

She, C. Y., and U. von Zahn (1998), Concept of a two-level mesopause: Support through new lidar observations, *J. Geophys. Res.*, *103*, 5855–5863, doi:10.1029/97JD03450.

She, C. Y., S. Chen, Z. Hu, J. Sherman, J. D. Vance, V. Vasoli, M. A. White, J. Yu, and D. A. Krueger (2000), Eight-year climatology of nocturnal temperature and sodium density in the mesopause region (80 to 105 km) over Fort Collins, Co (41°N, 105°W), *Geophys. Res. Lett.*, *27*, 3289–3292, doi:10.1029/2000GL003825.

Shepherd, M. G., W. F. J. Evans, G. Hernandez, D. Offermann, and H. Takahashi (2004), Global variability of mesospheric temperature: Mean temperature field, *J. Geophys. Res.*, *109*, D24117, doi:10.1029/2004JD005054.

Siva Kumar, V., Y. B. Kumar, K. Raghunath, P. B. Rao, M. Krishnaiah, K. Mizutani, T. Aoki, M. Yasui, and T. Itabe (2001), Lidar measurements of mesospheric temperature inversion at a low latitude, *Ann. Geophys.*, *19*, 1039–1044, doi:10.5194/angeo-19-1039-2001.

States, R. J., and C. S. Gardner (2000), Thermal structure of the mesopause region (80–105 km) at 40°N latitude. Part I: Seasonal variations, *J. Atmos. Sci.*, *57*, 66–77, doi:10.1175/1520-0469(2000)057<0066:TSOTMR>2.0.CO;2.

Thulasiraman, S., and J. B. Nee (2002), Further evidence of a two-level mesopause and its variations from UARS high-resolution Doppler imager temperature data, *J. Geophys. Res.*, *107*(D18), 4355, doi:10.1029/2000JD000118.

Torrence, C., and G. P. Compo (1998), A practical guide to wavelet analysis, *Bull. Am. Meteorol. Soc.*, *79*, 61–78, doi:10.1175/1520-0477(1998)079<0061:APGTWA>2.0.CO;2.

Venkat Ratnam, M., D. N. Rao, T. N. Rao, M. Krishnaiah, Y. B. Kumar, V. S. Kumar, and P. B. Rao (2002), Coordinated MST radar and lidar observations for the study of mesospheric structures over a tropical station, *J. Atmos. Sol. Terr. Phys.*, *64*, 349–358, doi:10.1016/S1364-6826(01)00101-8.

Venkat Ratnam, M., C. M. Shen, W. N. Chen, and J. B. Nee (2004), Study on oxygen atmospheric band dayglow: Global and seasonal variations deduced from high-resolution Doppler imager observations, *J. Atmos. Sol. Terr. Phys.*, *66*, 209–218, doi:10.1016/j.jastp.2003.10.009.

Venkat Ratnam, M., A. K. Patra, and B. V. Krishna Murthy (2010), Tropical mesopause: Is it always close to 100 km?, *J. Geophys. Res.*, *115*, D06106, doi:10.1029/2009JD012531.

von Zahn, U., J. Hoffner, V. Eska, and M. Alpers (1996), The mesopause altitude: Only two distinctive levels worldwide?, *Geophys. Res. Lett.*, *23*, 3231–3234, doi:10.1029/96GL03041.

Whiteway, J. A., A. I. Carswell, and W. E. Ward (1995), Mesospheric temperature inversions with overlying nearly adiabatic lapse rate: An indication of a well-mixed turbulent layer, *Geophys. Res. Lett.*, *22*, 1201–1204, doi:10.1029/95GL01109.

Xu, J., H. Liu, W. Yuan, A. K. Smith, R. G. Roble, C. J. Mertens, J. M. Russell, and M. G. Mlynczak (2007), Mesopause structure from Thermosphere, Ionosphere, Mesosphere, Energetics, and Dynamics (TIMED)/Sounding of the Atmosphere Using Broadband Emission Radiometry (SABER) observations, *J. Geophys. Res.*, *112*, D09102, doi:10.1029/2006JD007711.

U. Das and C. J. Pan, Institute of Space Science, National Central University, Jhongli 32001, Taiwan. (umadas@jupiter.ss.ncu.edu.tw)